

BosonSampling with single-photon Fock states from a bright solid-state source

J. C. Loredo,^{1,*} M. A. Broome,² P. Hilaire,^{3,4} O. Gazzano,⁵ I. Sagnes,³
A. Lemaitre,³ M. P. Almeida,¹ P. Senellart,^{3,6} and A. G. White¹

¹Centre for Engineered Quantum Systems, Centre for Quantum Computation and Communication Technology,
School of Mathematics and Physics, University of Queensland, Brisbane, Queensland 4072, Australia

²Centre of Excellence for Quantum Computation and Communication Technology,
School of Physics, University of New South Wales, Sydney, New South Wales 2052, Australia

³CNRS-LPN Laboratoire de Photonique et de Nanostructures,
Université Paris-Saclay, Route de Nozay, 91460 Marcoussis, France

⁴Université Paris Diderot-Paris 7, 75205 Paris CEDEX 13, France

⁵Joint Quantum Institute, National Institute of Standards and Technology,
University of Maryland, Gaithersburg, MD, USA

⁶Département de Physique, Ecole Polytechnique, Université Paris-Saclay, F-91128 Palaiseau, France

A BOSONSAMPLING device is a quantum machine expected to perform tasks intractable for a classical computer, yet requiring minimal non-classical resources as compared to full-scale quantum computers. Photonic implementations to date employed sources based on inefficient processes that only simulate heralded single-photon statistics when strongly reducing emission probabilities. BOSONSAMPLING with only single-photon input has thus never been realised. Here, we report on a BOSONSAMPLING device operated with a bright solid-state source of highly-pure single-photon Fock states: the emission from an efficient and deterministic quantum dot-micropillar system is demultiplexed into three partially-indistinguishable single-photons, with purity $1-g^{(2)}(0)$ of 0.990 ± 0.001 , interfering in a 6×6 linear optics network. Our demultiplexed source is orders-of-magnitude brighter than current heralded multi-photon sources based on spontaneous parametric down-conversion, allowing us to complete the BOSONSAMPLING experiment 100 times faster than previous equivalent implementations. This intrinsic source superiority places BOSONSAMPLING with larger photon numbers within near reach.

A core tenet of computer science is the Extended Church-Turing thesis, which states that all computational problems that are efficiently solvable by physically realistic machines are efficiently simulatable with classical resources. In 2011 Aaronson and Arkhipov introduced BOSONSAMPLING, a quantum protocol for efficiently sampling the output of a multimode bosonic interferometer [1–5]: a problem apparently intractable with classical computation. When scaled to many bosons this model of intermediate—i.e. non-universal—quantum computation will provide the strongest evidence against the Extended Church-Turing thesis.

The most experimentally accessible boson is the photon: to date full BOSONSAMPLING protocols have been performed using up to 4 photons [6–10]. These initial assays are well short of the numbers of single photons required to probe the Extended Church-Turing thesis: scalable photonic technology is required. The three core technologies needed for scalable quantum photonics are: single-photon sources [11–15]; large interferometric networks, with current integrated and programmable technology [16–19]; and efficient photon detection, with demonstrated number resolution [20, 21], and efficiencies of up to 95% [22].

Scaling of BOSONSAMPLING is primarily limited by photon sources. All implementations to date used photons obtained from spontaneous parametric down-conversion (SPDC), which is far from the ideal source of single-photon Fock states, $|\psi\rangle=|1\rangle$, instead produc-

ing primarily vacuum with a small admixture of pairs of photons, $|\psi\rangle=\sqrt{1-|\lambda|^2}\sum_{n=0}^{\infty}\lambda^n|nn\rangle$, where $|\lambda|\ll 1$. A *non-heralded* $2n$ -photon source can be built by using n down-converters, but it can only be used in specific protocols where the impact of higher photon-numbers is minimised [23]; conversely, it can be operated as a *heralded* n -photon source by detecting n photons—one from each down-converter—to herald the presence of their n single-photon partners. Multi-photon rates for state-of-the-art pulsed down-conversion sources [24–27], pumped at a standard 80 MHz repetition rate, range from ~ 300 kHz for 2 photons—yielding heralded single-photons at that rate—down to ~ 3 mHz for 8 photons—yielding 4 heralded single-photons at that rate. For as little as 6 heralded single-photons, the rate (~ 1 per year) becomes less than the detection rate of gravitational waves [28]. Using down-conversion to scale BOSONSAMPLING to many single-photons is clearly infeasible.

Quantum-dots in photonic structures [29–33] have been recently shown to produce long streams of indistinguishable single-photons with large emission yields [34, 35]. Efficient temporal-to-spatial demultiplexing of these sources will enable multi-photon experiments at scales heretofore impossible. Here we implement a BOSONSAMPLING device operated with a bright demultiplexed source of three highly-pure single-photon Fock states from the emission of a deterministic quantum dot-micropillar system [30]. The high source brightness allows us to complete the BOSONSAMPLING experiment

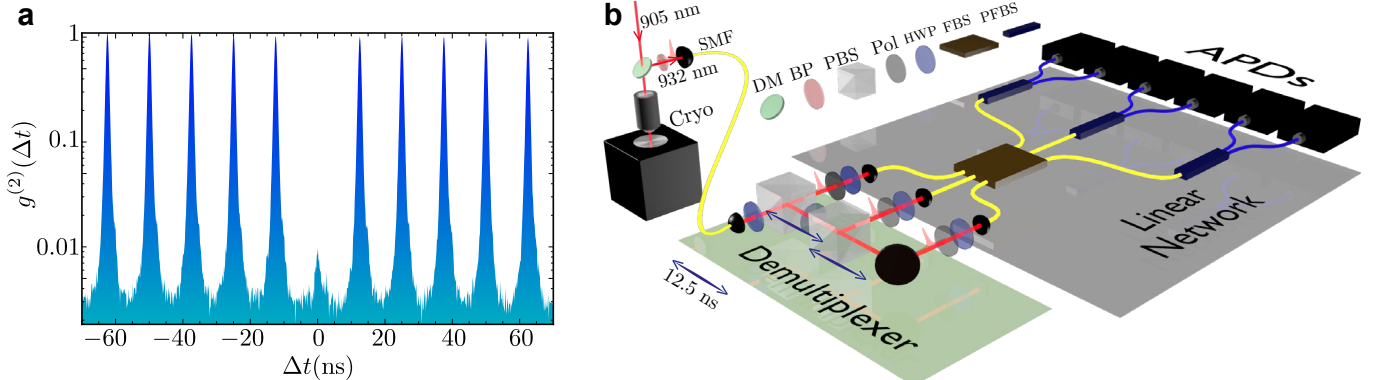


FIG. 1. **A BosonSampling device with pure single-photons.** (a) Second-order autocorrelation function $g^{(2)}(\Delta t)$ (log scale). A Hanbury Brown and Twiss experiment results in coincidences every $1/R_L=12.5$ ns: decreased detected events—antibunching—at $\Delta t=0$ indicates non-classical states of light. An ideal single-photon Fock state has $g^{(2)}(0)=0$; we measure $g^{(2)}(0)=0.010\pm 0.001$, resulting in a single-photon purity $1-g^{(2)}(0)$ of 0.990 ± 0.001 . (b) Experimental setup of BOSONSAMPLING with a solid-state single photon source. Laser pulses centred at 905 nm excite a quantum-dot embedded in a micropillar cavity, which itself is housed in an optically accessible cryostat (Cryo) system at 13 K. A dichroic mirror (DM), and band-pass filter (BP) with 0.85 nm FWHM are used to isolate the emitted single-photons at 932 nm collected in a single-mode fibre (SMF). A passive demultiplexer composed of beam-splitters with tunable transmittances—half-wave plates (HWP), and polarising beam-splitters (PBS)—and compensating delay lines of 12.5 ns probabilistically converts three consecutive single photons into separate spatial modes, where they are directed into the BOSONSAMPLING circuit. The scattering linear network is composed of polarisers (Pol), half-wave plates, a 3×3 non-polarising fibre beam-splitter (FBS), and polarising fibre beam-splitters (PFBS), which in combination form a 6×6 mode network [6]. Six avalanche photo-diodes (APDs) are used at the output to detect up to 3-fold coincidence events.

two orders-of-magnitude faster than in previous implementations. Our results prove solid-state sources an appealing candidate to constitute the basis for future quantum photonics, in particular for the implementation of BOSONSAMPLING with larger photon numbers.

Source of multiple single-photon Fock states. Laser pulses with a repetition rate of $R_L=80$ MHz and wavelength centred at 905 nm provide quasi-resonant excitation of an InGaAs quantum-dot deterministically coupled to a micropillar cavity, see refs. [30, 34] for a detailed description of this quantum dot-micropillar system. An optimised collection efficiency results in a record probability per pump-pulse of finding an spectrally-isolated single-photon at the output of a single-mode fiber—an absolute brightness—of up to $\eta_0=0.14$. As a result, our core source generates up to ~ 11 MHz of single-photons, modulo detector efficiencies, from which 3.6 MHz are detected with an avalanche photodiode (APD) of 32% quantum efficiency [34]. The absolute brightness depends on the laser pump power P according to $\eta=\eta_0(1-e^{-P/P_0})$, with $P_0=150$ μ W the saturation power. Under quasi-resonant excitation, single-photon sources based on non-gated quantum dots are subject to small and random frequency jitter—known as spectral diffusion—due to charges near the solid-state emitter [36, 37]. This results in the emission of photons with partial indistinguishability, which in our case is around 50–70% depending on the exact pump conditions [34]. These values are comparable to that in former BOSONSAMPLING experiments for photons from independent down-conversion events [6–10]. Our source

sees a small reduction in purity and indistinguishability with increasing pump power, we thus choose to operate it at $P=1.2P_0$. At this condition, it exhibits a single-photon purity $1-g^{(2)}(0)$ of 0.990 ± 0.001 , see Fig. 1a, where $g^{(2)}(\Delta t)$ is the second-order autocorrelation function, Δt is a time-lapse between two events defining a coincidence detection, and $g^{(2)}(0)=0$ holds for an ideal $|n\rangle=|1\rangle$ Fock state.

At this point, our source consists of sequentially emitted single-photons in orthogonal temporal modes within the same spatial mode. Our task now is to demultiplex it from the temporal to spatial domain, resulting in multiple orthogonal spatial modes containing a single-photon each with the same temporal mode, thus yielding a multiple single-photon source. This could be achieved with an active—temporally-varying—switcher, such that each of n consecutive single-photons is routed into a different spatial channel. Together with appropriate compensating delays, this results in a scalable method to demultiplex a photon source to multiple channels by optical switching.

A simpler alternative is to implement a passive demultiplexer, see Fig. 1b. Here, photon routing occurs by using an array of $n-1$ chained beam-splitters with tuned transmittances as to evenly distribute, with probability $1/n$, each single-photon into one of n possible outputs. The high absolute brightness in our core source allows us to readily operate sources of 2 and 3 single-photons. In Table I, we show the detected, and generated—corrected for detector efficiencies—count-rates of our demultiplexed n -photon source: n single-photons in the same temporal mode at the output of n single-mode fi-

n	Pump power	Detected rate	Detection efficiency, $(0.30)^n$	Generated rate
2	$3P_0$	15 kHz	9%	170 kHz
2	$1.2P_0$	9 kHz	9%	100 kHz
3	$3P_0$	50 Hz	2.7%	2 kHz
3	$1.2P_0$	20 Hz	2.7%	0.8 kHz

TABLE I. Demultiplexed n -photon count-rates. n -photon rates at high ($3P_0$) and medium ($1.2P_0$) pump powers detected with APDs of 0.30 average quantum efficiency. The generated rates take into account the n -photon detection efficiency of $(0.30)^n$.

bres.

The probabilistic demultiplexer is non-scalable, its success probability, modulo optical losses, scales as $1/n^n$; and the APD's quantum efficiency at these wavelengths is $\sim 30\%$. Remarkably, even when implemented with this passive demultiplexer and low-efficiency detectors, our count-rates meet those of high-purity non-heralded SPDC multi-photon sources [24–27]. Since our source intrinsically produces single—as opposed to twin—photons, a more relevant comparison is that to heralded SPDC single-photon rates. In this comparison, our source's detected and generated rates are respectively one and two orders-of-magnitude brighter, for both $n=2$, and $n=3$. (See ref. [38] for more details on our demultiplexed sources with both active and passive approaches).

Using this method, 2 and 3 partially-indistinguishable single-photons are used as inputs into a 6×6 fiber-based linear network \mathcal{L} consisting of 3 spatial- and 2 polarisation-encoded modes, see Fig. 1b. The relative temporal delay between photons is fine-tuned as to erase their temporal distinguishability, and the use of polarising fibre beam-splitters ensures that they are indistinguishable in polarisation.

BosonSampling with solid-state photon sources. We first input $N=2$ single-photons, and characterise the $M=6$ -mode \mathcal{L} network—in general a non-unitary transfer matrix due to inevitable optical losses—using the method described in ref. [39], see Supplementary Material. Following the theoretical model developed in ref. [40], 2 photons with a degree of indistinguishability quantified by \mathcal{I} , entering \mathcal{L} in inputs $\{i, j\}$ and exiting from outputs $\{k_1, k_2\}$ lead to a 2-fold coincidence probability:

$$p^{(2)} = \left(\frac{1 + \mathcal{I}}{2} \right) |\text{per}(\bar{\mathcal{L}})|^2 + \left(\frac{1 - \mathcal{I}}{2} \right) |\text{det}(\bar{\mathcal{L}})|^2, \quad (1)$$

given by the permanent (per) and determinant (det) of the submatrix $\bar{\mathcal{L}}$ formed with rows i, j and columns k_1, k_2 of \mathcal{L} . Note that Eq. (1) reduces to the well-known formula $p^{(2)} = |\text{per}(\bar{\mathcal{L}})|^2$ in the ideal case of perfect indistinguishability, i.e. $\mathcal{I}=1$.

We measured all $\binom{M}{N}=15$ outputs in which photons exit \mathcal{L} in different modes, so-called no-collision events. Peak areas in temporal-correlation measurements at these outputs allow us to extract—in a single experimental run—both the sampling distribution resulting from the Boson Sampler—that is, with partially-indistinguishable photons—and that of a (classical) distinguishable sampler arising from completely distinguishable particles. Given an output configuration k , coincidences detected under the area A_k^0 around zero delay $\Delta t=0$ are subject to two-photon interference: they determine the Boson Sampler distribution by measuring $\bar{p}_k^{(2)} = A_k^0$. Conversely, photons leading to coincidences around $\Delta t = \pm l \times (12.5 \text{ ns})$, for l integer, do not interfere, and one would expect that these distributions contain information of a classical sampler. Indeed, following ref. [34], one can deduce that the distinguishable sampler distribution is measured via $\bar{p}_k^{(2)}(0) = 2A_k^r - A_k^n - A_k^p$, where A_k^r is a reference area (average in grey peaks), A_k^n is the reduced area at negative Δt (left orange peak), and A_k^p is the reduced area at positive Δt (right orange peak) as shown in Fig. 2a. Measuring only no-collision events, however, does not provide access to the entire output distribution, thus to obtain probabilities we normalise the measured distributions to the corresponding theoretical prediction according to Eq. (1)—that is, the sum of experimentally obtained probabilities within the no-collision subspace is matched to that as in theory; and, given a 2-photon input $\{i, j\}$, $\mathcal{I}_{i,j}$ is extracted from the measured output distribution, see Supplementary Material.

Figure 2b shows our 2-photon BOSONSAMPLING results. Experimental distributions for the Boson Sampler (blue bars) are shown for 3 different 2-photon inputs, and their theoretical distributions (empty bars) are obtained with pair-wise indistinguishabilities $\mathcal{I}_{1,2}=0.520$, $\mathcal{I}_{2,3}=0.540$, and $\mathcal{I}_{1,3}=0.643$, respectively; in agreement with independently measured indistinguishabilities via two-photon interference on a 2×2 beamsplitter, see Supplementary Material. For the distinguishable sampler (red bars), the theoretical distribution (empty bars) is calculated by using $\mathcal{I}_{i,j}=0, \forall i, j$ in Eq. (1). To quantify the agreement between theory and experiment, we employ the statistical fidelity $\mathcal{F} = \sum_i \sqrt{p_i^{th} p_i^{exp}}$ between normalised theoretical and experimental distributions. For our 2-photon BOSONSAMPLING, we find an average fidelity of $\bar{\mathcal{F}}=0.9984 \pm 0.0007$ across the six sampled distributions in Fig. 2b, where the error here is one standard deviation among the six fidelity values.

We now tune the source to input $N=3$ single-photons into the $\{1, 2, 3\}$ mode. In this case, the probability of detecting a 3-fold coincidence at outputs of \mathcal{L} is [40]:

$$p^{(3)} = t_6^\dagger \left(\mathbb{I} + \sum_{i \neq j} \rho_{i,j} \mathcal{I}_{i,j} + \tilde{\rho} \prod_{i \neq j} \sqrt{\mathcal{I}_{i,j}} \right) t_6, \quad (2)$$

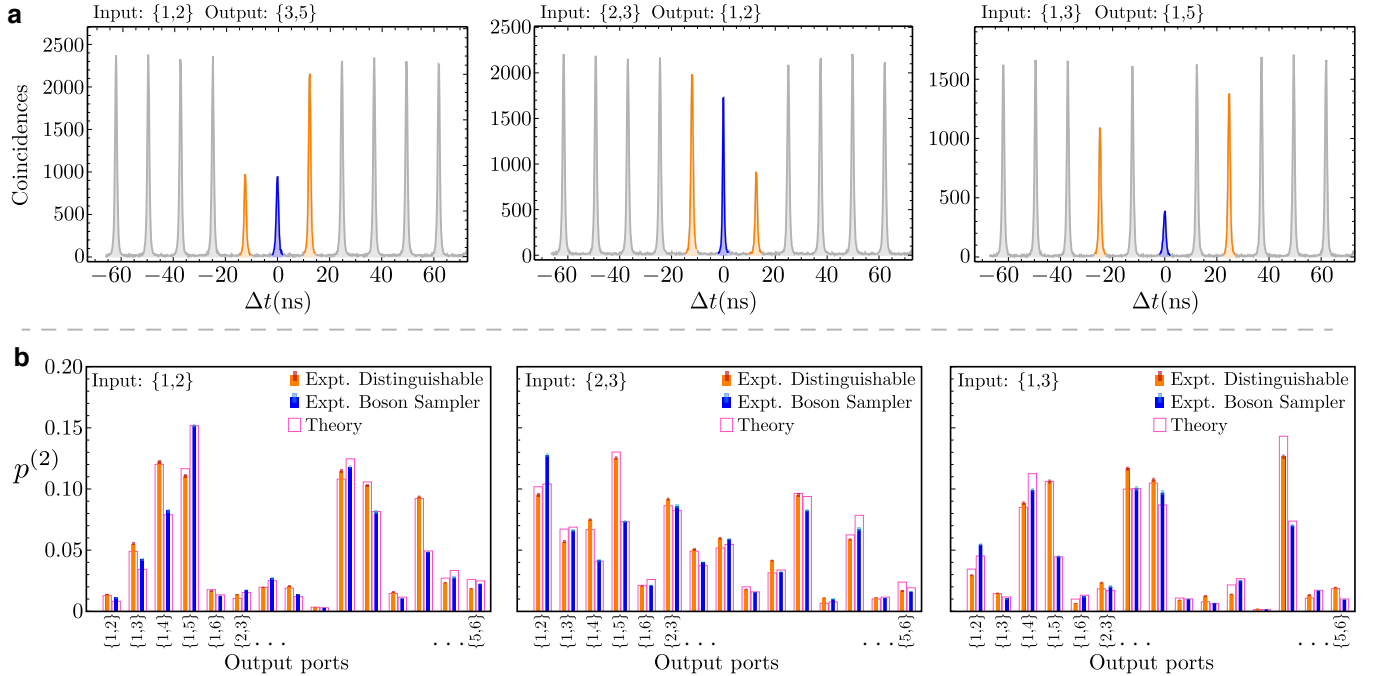


FIG. 2. Two-photon BOSONSAMPLING. (a) Temporal-correlation measurements at no-collision outputs for 2 photons entering at different inputs. Coincidences around $\Delta t=0$ (blue peaks) result from two-photon interference and are thus governed by Eq. (1). The position of reduced areas (orange peaks) indicates the temporal distance in emission from the quantum-dot: For inputs $\{1, 2\}$, and $\{2, 3\}$, photons were emitted after one laser repetition rate $1/R_L=12.5$ ns, thus reduced areas appear at $\pm 1/R_L$; similarly, appearing at ± 25 ns for $\{1, 3\}$, with photons emitted separated by 2 laser repetition rates. Coincidences outside $\Delta t=0$ (orange peaks and grey peaks) involve non-interfering photons, thus contain only classical information. (b) Coincidences at zero delay from the 15 no-collision outputs give the distribution of the Boson Sampler (blue bars), with theoretical distributions (empty bars) given by $I_{1,2}=0.520$, $I_{2,3}=0.540$, and $I_{1,3}=0.643$, for their respective input; whereas coincidences outside zero delay determine that of the distinguishable sampler (red bars), with theoretical distribution (empty bars) obtained by assuming zero indistinguishability in Eq. (1). Note that strong output configurations in the classical sampler *tend* to have a larger reduction when observed in the Boson Sampler. A complete sampled distribution is obtained with 10 minutes integration time; and, in average, a total of ~ 40000 2-fold events are collected for any given distribution. Error bars (small light-coloured bars) are deduced from assuming poissonian statistics in detected events.

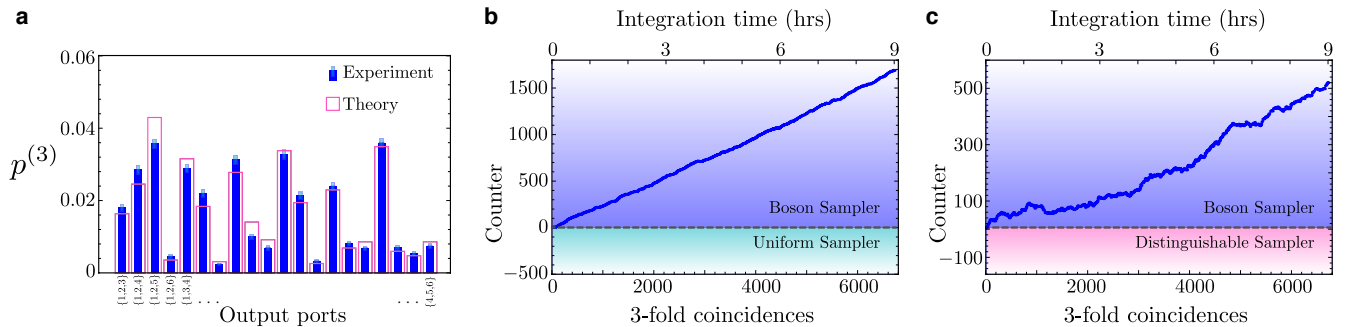


FIG. 3. Three-photon BOSONSAMPLING. (a) A total of 20 no-collision 3-fold simultaneous coincidences are recorded to obtain the Boson Sampler distribution (blue bars); the theoretical distribution (empty bars) is obtained from Eq. (2) and by using the previously determined pair-wise indistinguishability parameters. Error bars (light-coloured bars) are deduced from poissonian statistics in measured events. We apply the validation of BOSONSAMPLING protocol against the uniform sampler (b), and distinguishable sampler (c). A counter (blue dots) is updated for every 3-fold event and at any point a positive value validates the data as being obtained from a BOSONSAMPLER as opposed to either a uniform or distinguishable sampler, see Methods. The final data set contains a total of 6725 3-fold events collected in 9 hours, that is ~ 1000 per 80 minutes; outperforming previous BOSONSAMPLING experiments with 3-fold rates of ~ 1000 per 100 hours.

with \mathbb{I} , the 6×6 identity operator; t_6 , a 6-component quantity that depends on the permanent, determinant, and immanants of 3×3 submatrices \mathcal{T} ; and the $\rho_{i,j}$, and $\tilde{\rho}$ matrices as explicitly defined in the Supplementary Material. Eq. (2) reduces to $p^{(3)} = |\text{per}(\mathcal{T})|^2$ in the ideal case of perfect indistinguishability between all particles, i.e. $\mathcal{I}_{i,j} = 1, \forall i, j$.

Verifying the output distribution of a BOSONSAMPLING device involves calculating a number of (modulus squared) matrix permanents. This task is in general computationally hard to implement efficiently on a classical computer. The complete result of a large-scale BOSONSAMPLING machine is thus likely to be, even in principal, unverifiable. It has been even argued that a large-scale BOSONSAMPLING experiment will fail to distinguish its data from the (trivial) uniform distribution—i.e., one in which every output configuration is equally probable [41]. In light of this, some methods have been proposed and demonstrated for the *validation* of BOSONSAMPLING: circumstantial evidence is provided to support that a BOSONSAMPLING machine is indeed functioning according to the laws of quantum mechanics, by ruling out that the experimentally obtained data originates from, e.g., the uniform distribution, or a sampler with distinguishable particles [19, 42–44]. These protocols are scalable: it is not needed to observe all output configurations, which grow exponentially with system size, instead even modest numbers of multi-fold detected events reveal the sampling nature of a device.

Figure 3 shows our experimental results for the 3-photon Boson Sampler. In Fig. 3a, the previously determined 2-photon indistinguishabilities $\mathcal{I}_{i,j}$ are used as input for the theoretical distribution (empty bars) according to Eq. (2), and experimental probabilities (blue bars) are obtained by measuring the $\binom{M}{N} = 20$ 3-fold simultaneous—i.e. around $\Delta t = 0$ —coincidences for no-collision events normalised to the theoretical prediction. In this case, we find the 3-photon BOSONSAMPLING fidelity $\mathcal{F} = 0.997 \pm 0.006$, where the error here results from propagated poissonian statistics. In Figs. 3b,c, we apply the validation of BOSONSAMPLING protocol to our data. We record 3-fold coincidences in steps of 30 seconds, in which time a counter is updated. For each detected 3-fold coincidence, the counter is either increased or decreased in one unit, and it is designed, see Methods, such that after an experimental run a positive value validates the data as obtained from the Boson Sampler distribution, whereas a negative counter indicates it originates from the uniform sampler, see Fig. 3b, or the distinguishable sampler, see Fig. 3c.

Discussion

We experimentally demonstrated multi-photon interference with a highly-efficient solid-state source: A BOSONSAMPLING device implemented with single-photon Fock states emitted by a deterministic quantum

dot-micropillar system. The drastically high efficiency of our source allowed us to sample interferometric multimode outputs in time-scales 2 orders-of-magnitude faster than in previous experiments with SPDC sources: a representative number of 1000 3-fold sampled events, obtained in ~ 100 hours in previous experiments [6–9], were collected here in 80 minutes. This performance is attained despite using detectors with half the efficiency of those at down-conversion wavelengths, and an inherently inefficient demultiplexing approach.

We have directly observed the effect of partial distinguishability: Our results follow closely the sampling of permanents and immanants of matrices with contributions weighted by pair-wise degrees of indistinguishability. Moreover, by exploiting temporal-correlation measurements we showed that both classical and quantum 2-photon sampling distributions can be obtained simultaneously, which can be readily extended to multi-fold temporal-dependent measurements in a larger BOSONSAMPLING experiment. Potentially, this could motivate new validation protocols exploiting statistics that include this temporal degree of freedom.

The impact of partial distinguishability in BOSONSAMPLING has been studied theoretically [40, 45, 46], and reported experimentally [40]. However, identifying experimentally this property in isolation is challenging. Previous experiments with down-conversion exhibit photon-statistics polluted by higher-order terms [23], which can be mistakenly interpreted as decreased photon-indistinguishability. In fact, in many cases these higher-order terms, and not photon distinguishability, are the main cause of performance degradation in SPDC-based protocols [47, 48]. The pathway to maximise indistinguishability in efficient solid-state sources is well known: resonant excitation of the quantum-dot results in near-optimal values of photon indistinguishability [32, 33], in which case the obtained output distributions will be close to the sampling of only permanents—functions belonging to the #P complexity class, in which the main complexity arguments of BOSONSAMPLING apply.

We believe our results pave the way to the forthcoming advent of quantum-dot based quantum photonics, in which a future BOSONSAMPLING implementation with efficiently demultiplexed and resonantly-pumped solid-state sources may finally see the Extended Church-Turing thesis put to serious test.

Methods

Validation of BosonSampling. Aaronson and Arkhipov proposed a protocol to test data against the uniform sampler [42], as a counterargument to the claim [41] that a large-scale BOSONSAMPLING implementation would fail to distinguish the experimental data even from that of the trivial one. The method—used in Fig. 3b—exploits available information of the sampling device—the transfer matrix \mathcal{L} —to define an estimator

$P_{\text{est}} = \prod_{i=1}^n \sum_{j=1}^n |\bar{\mathcal{L}}_{i,j}|^2$, with $\bar{\mathcal{L}}_{i,j}$ the $n \times n$ submatrix of the $m \times m$ transfer matrix in an experiment involving n bosons in m modes. Unlike the permanent, P_{est} is efficiently computable—thus, the protocol is scalable—and yet is correlated with the Boson Sampler probabilities. For the uniform distribution, the probability of one photon entering \mathcal{L} in input i and exiting in output j is a constant (uniform) value $|\bar{\mathcal{L}}_{i,j}|^2 = 1/m$ across any input/output setting, thus the estimator takes the form $P_{\text{est}}^u = (n/m)^n$. If the sampling device is functioning correctly, one expects to observe more probable events more often; thus the method simply consists of computing P_{est} for every event observed, and keeping track of a counter that is increased in one unit if $P_{\text{est}} > P_{\text{est}}^u$, and decreased in one unit otherwise. A resulting positive counter then validates the BOSONSAMPLING experiment by rejecting the hypothesis that the data originates from the uniform sampler. Experimental evidence supporting that this method works, even with small data samples and experimental imperfections, was reported in refs. [43, 44].

A different protocol to test the data against a distinguishable sampler was proposed and demonstrated by Spagnolo et. al. [43]. This method—used in Fig. 3c—exploits a key difference between sampling distinguishable or indistinguishable bosons: bosonic bunching. Output configurations, within the no-collision space, that are strong in classical distributions tend to have a larger reduction in probability when observed in the quantum regime. As a result, the relative—i.e., normalised in the no-collision space—probabilities p^Q that are higher within the quantum regime tend to be also numerically higher than that probability in the classical regime p^C : if the data originates from a Boson Sampler one tends to observe more configurations with $p^Q > p^C$. The method then consists on computing p^Q , and p^C for every event observed and keeping track of a counter increased in one unit if $p^Q > p^C$, and decreased in one unit otherwise. At the end of an experimental run a positive counter validates a correct functioning of the BOSONSAMPLING machine by rejecting the distinguishable sampler hypothesis. The method is scalable: although it involves classically computing permanents in p^Q , this only needs to be done for a limited number of observed events, and not for the exponentially growing configurations of the entire output distribution.

* Corresponding author: juan.loredo1@gmail.com

[1] S. Aaronson and A. Arkhipov, Proc. ACM Symposium on Theory of Computing, San Jose, CA , 333 (2011).

[2] S. Aaronson, Proceedings of the Royal Society A: Mathematical, Physical and Engineering Science **467**, 3393 (2011).

[3] C. Shen, Z. Zhang, and L.-M. Duan, Phys. Rev. Lett. **112**, 050504 (2014).

[4] A. P. Lund et al., Phys. Rev. Lett. **113**, 100502 (2014).

[5] J. Huh, G. G. Guerreschi, B. Peropadre, J. R. McClean, and A. Aspuru-Guzik, Nat Photon **9**, 615 (2015).

[6] M. A. Broome et al., Science **339**, 794 (2013).

[7] J. B. Spring et al., Science **339**, 798 (2013).

[8] M. Tillmann et al., Nat Photon **7**, 540 (2013).

[9] A. Crespi et al., Nat Photon **7**, 545 (2013).

[10] M. Bentivegna et al., Science Advances **1** (2015).

[11] P. G. Kwiat, E. Waks, A. G. White, I. Appelbaum, and P. H. Eberhard, Phys. Rev. A **60**, 773 (1999).

[12] T. Pittman, B. Jacobs, and J. Franson, Optics communications **246**, 545 (2005).

[13] T. M. Babinec et al., Nature nanotechnology **5**, 195 (2010).

[14] Z. Yuan et al., Science **295**, 102 (2002).

[15] C. Santori, D. Fattal, J. Vučković, G. S. Solomon, and Y. Yamamoto, Nature **419**, 594 (2002).

[16] A. Politi, M. J. Cryan, J. G. Rarity, S. Yu, and J. L. O'Brien, Science **320**, 646 (2008).

[17] B. J. Smith, D. Kundys, N. Thomas-Peter, P. G. R. Smith, and I. A. Walmsley, Opt. Express **17**, 13516 (2009).

[18] A. Crespi et al., Nat Commun **2**, 566 (2011).

[19] J. Carolan et al., Science **349**, 711 (2015).

[20] A. J. Miller, S. W. Nam, J. M. Martinis, and A. V. Sergienko, Applied Physics Letters **83**, 791 (2003).

[21] A. Divochi et al., Nature Photonics **2**, 302 (2008).

[22] A. E. Lita, A. J. Miller, and S. W. Nam, Opt. Express **16**, 3032 (2008).

[23] J.-W. Pan et al., Rev. Mod. Phys. **84**, 777 (2012).

[24] X.-C. Yao et al., Nat Photon **6**, 225 (2012).

[25] B. J. Metcalf et al., Nat Commun **4**, 1356 (2013).

[26] C. Zhang et al., Phys. Rev. Lett. **115**, 260402 (2015).

[27] J. C. Loredo et al., Phys. Rev. Lett. **116**, 070503 (2016).

[28] B. P. Abbott et al., Phys. Rev. Lett. **116**, 061102 (2016).

[29] P. Lodahl et al., Nature **430**, 654 (2004).

[30] O. Gazzano et al., Nature communications **4**, 1425 (2013).

[31] P. Lodahl, S. Mahmoodian, and S. Stobbe, Rev. Mod. Phys. **87**, 347 (2015).

[32] X. Ding et al., Phys. Rev. Lett. **116**, 020401 (2016).

[33] N. Somaschi et al., arXiv:1510.06499 (2016).

[34] J. C. Loredo et al., arXiv:1601.00654 (2016).

[35] H. Wang et al., arXiv:1602.07386 (2016).

[36] A. V. Kuhlmann et al., Nat Phys **9**, 570 (2013).

[37] S. Unsleber et al., Phys. Rev. B **91**, 075413 (2015).

[38] J. C. Loredo et al., Manuscript in preparation (2016).

[39] S. Rahimi-Keshari et al., Opt. Express **21**, 13450 (2013).

[40] M. Tillmann et al., Phys. Rev. X **5**, 041015 (2015).

[41] C. Gogolin, M. Kliesch, L. Aolita, and J. Eisert, arXiv:1306.3995 (2013).

[42] S. Aaronson and A. Arkhipov, arXiv:1309.7460 (2013).

[43] N. Spagnolo et al., Nat Photon **8**, 615 (2014).

[44] J. Carolan et al., Nat Photon **8**, 621 (2014).

[45] V. S. Shchesnovich, Phys. Rev. A **91**, 013844 (2015).

[46] M. C. Tichy, Phys. Rev. A **91**, 022316 (2015).

[47] T. J. Weinhold et al., arXiv:0808.0794 (2008).

[48] M. Barbieri et al., Journal of Modern Optics **56**, 209 (2009).

Acknowledgements

This work was partially supported by the Centre for Engineered Quantum Systems (Grant No. CE110001013), the Centre for Quantum Computation and Communication Technology (Grant No. CE110001027), the Asian Office of Aerospace Research and Development (grant FA2386-13-1-4070), by the ERC Starting Grant No. 277885 QD-CQED, the French Agence Nationale pour la Recherche (ANR DELIGHT, ANR USSEPP), the French RENATECH network, the Labex NanoSaclay. A.G.W. acknowledges support from a UQ Vice-Chancellors Research and Teaching Fellowship. J.C.L., M.P.A., and A.G.W. thank the team from the Austrian Institute of Technology for kindly providing time-tagging modules, and Devon Biggerstaff for experimental assistance. J.C.L. thanks Saleh Rahimi-Keshari, Marco Bentivegna, and Fabio Sciarrino for useful discussions.

Author contributions

Installation of the quantum-dot sample in the lab was conducted by O.G., M.P.A., and M.A.B. The sample was grown by A.L., and the etching performed by I.S. The experiment was performed by J.C.L., with help from P.H. The paper was written by J.C.L., with help from M.A.B., and edited by A.G.W., and P.S. The project was conceived by A.G.W., and supervised by A.G.W. and P.S.

SUPPLEMENTARY MATERIAL

I. Transfer matrix

The linear network is characterised with the method introduced in ref. [39]. For all measurements presented in the main text, inputs 1, 2, and 3 of \mathcal{L} are used. The transfer matrix \mathcal{L} in this subspace is given by:

$$\mathcal{L} = \begin{bmatrix} 0.314 & 0.160 & 0.251 & 0.578 & 0.576 & 0.188 \\ 0.561 & -0.157 + 0.151i & -0.319 + 0.440i & -0.388 - 0.033i & 0.331 - 0.127i & -0.120 - 0.226i \\ 0.473 & 0.352 + 0.409i & -0.054 - 0.025i & 0.249 - 0.206i & -0.559 + 0.112i & 0.085 - 0.118i \end{bmatrix}, \quad (3)$$

where the element $\mathcal{L}_{i,j}$ represents the probability amplitude for a photon entering \mathcal{L} in input i and exiting in output j .

II. Pair-wise indistinguishability

We obtain the degrees of pair-wise indistinguishability $\mathcal{I}_{i,j}$ between photons at inputs $\{i, j\}$ by minimising the variation distance $d=1/2 \sum_k |p_k^{(2),\text{exp}} - p_k^{(2),\text{th}}|$ between experimental and theoretical distributions. As described in the main text, $p^{(2),\text{exp}}$ is normalised to $\sum_k p_k^{(2),\text{th}}$. This being relevant when computing d as distributions for different degrees of indistinguishability have different normalisation factors. For a given 2-photon input $\{i, j\}$, $\mathcal{I}_{i,j}$ is taken as that at the global minimum in d . We obtain $\mathcal{I}_{1,2}=0.520$, $\mathcal{I}_{2,3}=0.540$, and $\mathcal{I}_{1,3}=0.643$, see Fig.S 4.

We carried out time-correlated measurements of two-photon interference on a 2×2 beam-splitter to independently verify these degrees of indistinguishability. It has been shown in ref. [34] that the indistinguishability of two photons emitted by a semiconductor quantum dot depends on their emission temporal distance Δt_e . When both photons are emitted with the same polarisation from the quantum dot, their indistinguishability decreases monotonically in Δt_e . In our case we obtain $\mathcal{I}_{12,5\text{ns}}^{bs}=0.6360 \pm 0.0063$ for photons emitted with $\Delta t_e=12.5$ ns, and $\mathcal{I}_{25\text{ns}}^{bs}=0.6252 \pm 0.0065$ for $\Delta t_e=25$ ns,

see Fig.S 5. Note that for these measurements photons are emitted with the same polarisation from the quantum dot.

The amount of indistinguishability $\mathcal{I}_{1,3}=0.643$, involving photons emitted with $\Delta t_e=25$ ns, and $\mathcal{I}_{25\text{ns}}^{bs}=0.6252 \pm 0.0065$ are in good agreement. Both $\mathcal{I}_{1,2}=0.520$, and $\mathcal{I}_{2,3}=0.540$ involve photons emitted with $\Delta t_e=12.5$ ns, therefore the minimisation method finds similar values, these however present a slight discrepancy with $\mathcal{I}_{12,5\text{ns}}^{bs}=0.6360 \pm 0.0063$. The quantum dot presents a small fine structure splitting of the exciton line, which in turn reduces the indistinguishability of photons emitted from two orthogonal emissions. Inputs $\{1, 2\}$, and $\{2, 3\}$ in the BOSONSAMPLING experiment contain photons separated by the first polarising beam-splitter in the source demultiplexer (see main text), thus they are emitted with orthogonal polarisations from the quantum dot and exhibit a reduced value of indistinguishability compared to photons emitted with the same polarisation, in agreement with the obtained values.

III. Three-photon interference

We employ the theoretical model introduced in ref. [40] to describe the interference of 3 photons, labeled 1, 2, and 3, scattered across a linear network \mathcal{L} . In such case, the probability of detecting a 3-fold coincidence at the output $\{o_1, o_2, o_3\}$ of \mathcal{L} is:

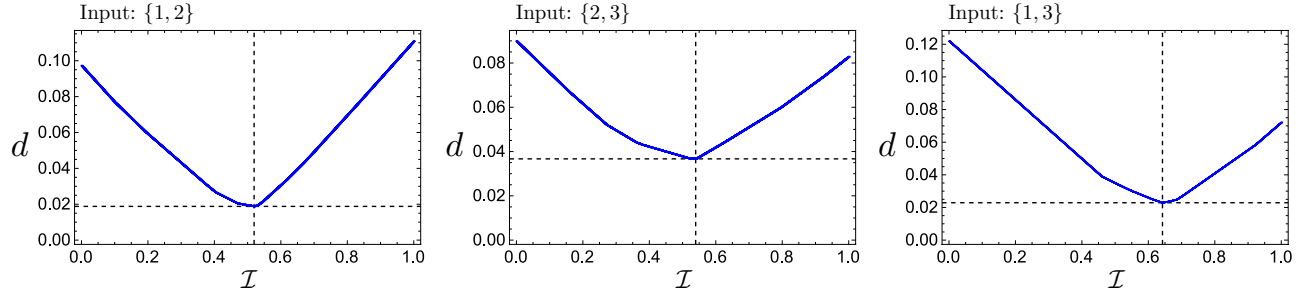


FIG. 4. Variation distance d between experimental and theoretical distributions. d is a global minimum at $\mathcal{I}_{1,2}=0.520$, $\mathcal{I}_{2,3}=0.540$, and $\mathcal{I}_{1,3}=0.643$ for its corresponding 2-photon input. The variation distances at these points are respectively $d_{1,2}=0.019$, $d_{2,3}=0.037$, and $d_{1,3}=0.023$. These values are obtained with both experimental and theoretical distributions normalised to the non-unity theoretical normalisation factor. When the distributions are normalised to unity, the variation distances are $d_{1,2}=0.028$, $d_{2,3}=0.049$, and $d_{1,3}=0.055$, respectively.

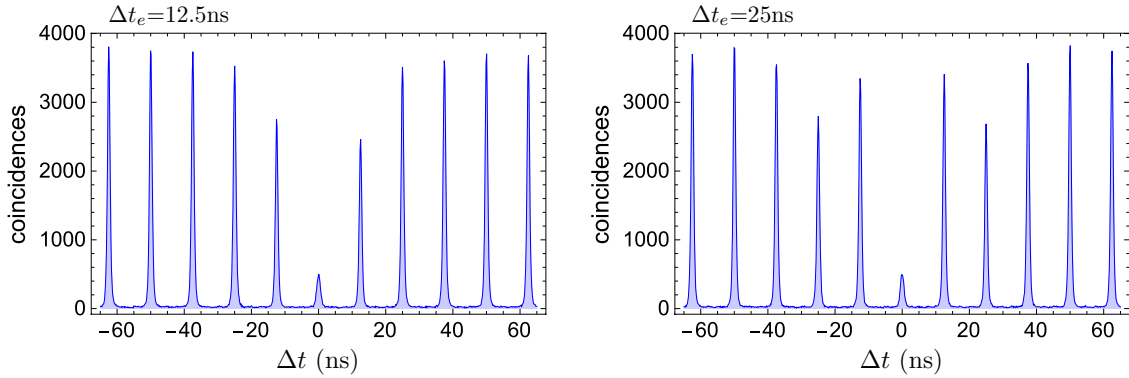


FIG. 5. Two-photon interference on a 2×2 beam-splitter. Temporal-correlation measurements result in a series of peaks from which the degree of indistinguishability can be directly extracted via $\mathcal{I}=(R^2+T^2-A_0/A)/(2RT)$, with $R=0.471$ the beam-splitter reflectance, $T=1-R$, A the average peak area outside $\Delta t=0$ (excluding reduced peaks at Δt_e), and A_0 the peak area around $\Delta t=0$. See ref. [34] for a derivation of this formula. We obtain $\mathcal{I}_{12.5\text{ns}}^{bs}=0.6360\pm 0.0063$ for $\Delta t_e=12.5$ ns, and $\mathcal{I}_{25\text{ns}}^{bs}=0.6252\pm 0.0065$ for $\Delta t_e=25$ ns. Errors are estimated from propagated poissonian statistics.

$$p^{(3)} = t_6^\dagger \left(\mathbb{I} + \rho_{1,2} \mathcal{I}_{1,2} + \rho_{2,3} \mathcal{I}_{2,3} + \rho_{1,3} \mathcal{I}_{1,3} + \tilde{\rho} \sqrt{\mathcal{I}_{1,2}} \sqrt{\mathcal{I}_{2,3}} \sqrt{\mathcal{I}_{1,3}} \right) t_6; \quad (4)$$

where

$$t_6 = \begin{pmatrix} \frac{1}{\sqrt{6}} \text{per}(\mathcal{T}) \\ \frac{1}{\sqrt{6}} \text{det}(\mathcal{T}) \\ \frac{1}{2\sqrt{3}} \text{imm}(\mathcal{T}) + \frac{1}{2\sqrt{3}} \text{imm}(\mathcal{T}_{213}) \\ \frac{1}{6} \text{imm}(\mathcal{T}) - \frac{1}{3} \text{imm}(\mathcal{T}_{132}) - \frac{1}{6} \text{imm}(\mathcal{T}_{213}) + \frac{1}{3} \text{imm}(\mathcal{T}_{312}) \\ \frac{1}{6} \text{imm}(\mathcal{T}) + \frac{1}{3} \text{imm}(\mathcal{T}_{132}) + \frac{1}{6} \text{imm}(\mathcal{T}_{213}) + \frac{1}{3} \text{imm}(\mathcal{T}_{312}) \\ -\frac{1}{2\sqrt{3}} \text{imm}(\mathcal{T}) + \frac{1}{2\sqrt{3}} \text{imm}(\mathcal{T}_{213}) \end{pmatrix},$$

$$\mathbb{I} = \begin{pmatrix} 1 & 0 & 0 & 0 & 0 & 0 \\ 0 & 1 & 0 & 0 & 0 & 0 \\ 0 & 0 & 1 & 0 & 0 & 0 \\ 0 & 0 & 0 & 1 & 0 & 0 \\ 0 & 0 & 0 & 0 & 1 & 0 \\ 0 & 0 & 0 & 0 & 0 & 1 \end{pmatrix}, \quad \rho_{1,2} = \begin{pmatrix} 1 & 0 & 0 & 0 & 0 & 0 \\ 0 & -1 & 0 & 0 & 0 & 0 \\ 0 & 0 & 1 & 0 & 0 & 0 \\ 0 & 0 & 0 & -1 & 0 & 0 \\ 0 & 0 & 0 & 0 & 1 & 0 \\ 0 & 0 & 0 & 0 & 0 & -1 \end{pmatrix}, \quad \rho_{2,3} = \begin{pmatrix} 1 & 0 & 0 & 0 & 0 & 0 \\ 0 & -1 & 0 & 0 & 0 & 0 \\ 0 & 0 & -\frac{1}{2} & -\frac{\sqrt{3}}{2} & 0 & 0 \\ 0 & 0 & -\frac{\sqrt{3}}{2} & \frac{1}{2} & 0 & 0 \\ 0 & 0 & 0 & 0 & -\frac{1}{2} & -\frac{\sqrt{3}}{2} \\ 0 & 0 & 0 & 0 & -\frac{\sqrt{3}}{2} & \frac{1}{2} \end{pmatrix},$$

$$\rho_{1,3} = \begin{pmatrix} 1 & 0 & 0 & 0 & 0 & 0 \\ 0 & -1 & 0 & 0 & 0 & 0 \\ 0 & 0 & -\frac{1}{2} & \frac{\sqrt{3}}{2} & 0 & 0 \\ 0 & 0 & \frac{\sqrt{3}}{2} & \frac{1}{2} & 0 & 0 \\ 0 & 0 & 0 & 0 & -\frac{1}{2} & \frac{\sqrt{3}}{2} \\ 0 & 0 & 0 & 0 & \frac{\sqrt{3}}{2} & \frac{1}{2} \end{pmatrix}, \quad \tilde{\rho} = \begin{pmatrix} 2 & 0 & 0 & 0 & 0 & 0 \\ 0 & 2 & 0 & 0 & 0 & 0 \\ 0 & 0 & -1 & 0 & 0 & 0 \\ 0 & 0 & 0 & -1 & 0 & 0 \\ 0 & 0 & 0 & 0 & -1 & 0 \\ 0 & 0 & 0 & 0 & 0 & -1 \end{pmatrix},$$

$\mathcal{I}_{1,2}$, $\mathcal{I}_{2,3}$, and $\mathcal{I}_{1,3}$ are pair-wise indistinguishability values; \mathcal{T} is a 3×3 submatrix built with rows 1, 2, and 3, and columns o_1 , o_2 , and o_3 of \mathcal{L} ; $\mathcal{T}_{a,b,c}$ is the matrix \mathcal{T} with rows 1, 2, and 3 rearranged in order o_1 , o_2 , and o_3 ; and the permanent (per), determinant (det), and immanant

(imm) of a 3×3 matrix are defined as:

$$\begin{aligned} \text{per} \begin{pmatrix} a & b & c \\ d & e & f \\ g & h & i \end{pmatrix} &= aei + bfg + cdh + ceg + bdi + afh, \\ \text{det} \begin{pmatrix} a & b & c \\ d & e & f \\ g & h & i \end{pmatrix} &= aei + bfg + cdh - ceg - bdi - afh, \\ \text{imm} \begin{pmatrix} a & b & c \\ d & e & f \\ g & h & i \end{pmatrix} &= 2aei - bfg - cdh. \end{aligned}$$